Self-organized biotectonics of termite nests

Alexander Heyde[a], Lijie Guo[b], Christian Jost[b], Guy Theraulaz[b], and L. Mahadevan[a,c,d,1]

[a]Department of Organismic and Evolutionary Biology, Harvard University, Cambridge, MA 02138; [b]Centre de Recherches sur la Cognition Animale, Centre de Biologie Intégrative, Université de Toulouse, CNRS, Université de Toulouse–Paul Sabatier, 31062 Toulouse France; [c]School of Engineering and Applied Sciences, Harvard University, Cambridge, MA 02138; and [d]Department of Physics, Harvard University, Cambridge, MA 02138

Edited by Simon A. Levin, Princeton University, Princeton, NJ, and approved November 16, 2020 (received for review April 16, 2020)

The termite nest is one of the architectural wonders of the living world, built by the collective action of workers in a colony. Each nest has several characteristic structural motifs that allow for efficient ventilation, cooling, and traversal. We use tomography to quantify the nest architecture of the African termite *Apicotermes lamani*, consisting of regularly spaced floors connected by scattered linear and helicoidal ramps. To understand how these elaborate structures are built and arranged, we formulate a minimal model for the spatiotemporal evolution of three hydrodynamic fields—mud, termites, and pheromones—linking environmental physics to collective building behavior using simple local rules based on experimental observations. We find that floors and ramps emerge as solutions of the governing equations, with statistics consistent with observations of *A. lamani* nests. Our study demonstrates how a local self-reinforcing biotectonic scheme is capable of generating an architecture that is simultaneously adaptable and functional, and likely to be relevant for a range of other animal-built structures.

collective animal behavior | termite nests | stigmergy | ecophysiology | morphogenesis

Termite nests are among the most complex and impressive structures produced by animal societies (1–3) and serve to create a microniche that allows for the controllable exchange of matter and energy with the environment (4–6). Even when compared with the many animal species that exhibit collective behaviors, including coordinated motion, active synchronization, or shared decision making (7, 8), the collective activities of social insects such as the highly eusocial termite are exceptional, in that they often lead to the formation of intricate physical structures: shelters (9); trail networks (10); and, most prominently, nests (1, 2). These structures are not merely the byproduct of animal behavior, however, since they also play a central role in regulating the flow of information necessary for their own construction and function. Nest building in social insects is thus considered an exemplar of functional self-organization, and studying this process can inform us about how structure and function emerge in ecophysiology (11).

The eusocial termites of the genus *Apicotermes* typify the architectural complexity that can be produced by social insects. These termites, native to the savannahs and forests of Africa, construct small ovoid nests just 20 to 40 cm in diameter, located 5 to 50 cm underground (12). The nest structure must be efficiently constructed to be capable of passive ventilation and cooling (4–6, 13–15), while remaining habitable and traversable by the termites within. This is no small feat—given the scale and complexity of *Apicotermes* nests, it is not feasible that any single termite has a sufficiently broad cognitive map of the organization of the whole structure to coordinate the actions of the colony (16). Yet even in the absence of centralized control, these nests clearly show coherent structure at a global scale, pointing to the collective self-organization of several thousand termites acting only on their local conditions to produce global order (3, 11, 16).

Rather than termites sharing information by direct communication (such as via antennal contact or gestures), Grassé (17) proposed that termite workers communicate indirectly by coupling their building actions with the deposition of a local stimulus (such as a secreted building pheromone) in nearby substrate. This principle of stigmergy—defined as the spontaneous but indirect coordination of agents stimulated to action by the trace of previous actions left in the environment (16)—has already been implicated in the morphogenesis of the large structures that enclose the nest. Over the long length and time scales of the overall mound structure, the small internal tunnels and chambers within the mound influence the mound material porosity (2, 15); mediate ventilation (5, 6); and suffice to explain the coarse features of the mound, such as its shape, size, and temporal evolution (18).

However, this leaves open questions of how the internal structural motifs are formed and maintained at shorter length scales in the mound microstructure. These questions have only recently begun to be addressed in other insects, like in the far simpler structures of the ant *Lasius niger* (19), typically with computationally expensive individual-based modeling rather than continuum approaches. Overall, the comparatively more complex architecture of *Apicotermes* nests begs two important questions: First, what are the structural motifs within the nest, and how are they arranged? And second, how are they formed via the dynamic feedback loop between individual behavior and emerging structure in the nest construction process?

Digitization and Structure of *Apicotermes* Nests

To answer these questions, we first collected, scanned, and statistically analyzed the structure of nests in the species *Apicotermes lamani*. Two nests (MeMo14, Fig. 1*A*, and MeMo13, Fig. 1*B*)

Significance

Termite nests are a remarkable example of functional self-organization that show how structure and function emerge on multiple length and time scales in ecophysiology. To understand the process by which this arises, we document the labyrinthine architecture within the subterranean nests of the African termite *Apicotermes lamani* and develop a simple mathematical model that relies on the physical and biological interactions between termites, pheromones, and mud in the nest. Our model explains the formation of parallel floors connected by linear and helical ramps, consistent with observations of real nests. In describing this multiagent system, we elucidate principles of physical and behavioral coupling with relevance to swarm intelligence and architectural design.

Author contributions: A.H., G.T., and L.M. designed research; A.H. and L.M. performed research; A.H., L.G., C.J., G.T., and L.M. contributed new reagents/analytic tools; A.H., L.G., C.J., and L.M. analyzed data; and A.H., G.T., and L.M. wrote the paper.

The authors declare no competing interest.

This article is a PNAS Direct Submission.

[1]To whom correspondence may be addressed. Email: lmahadev@g.harvard.edu.

This article contains supporting information online at https://www.pnas.org/lookup/suppl/doi:10.1073/pnas.2006985118/-/DCSupplemental.

Published January 18, 2021.

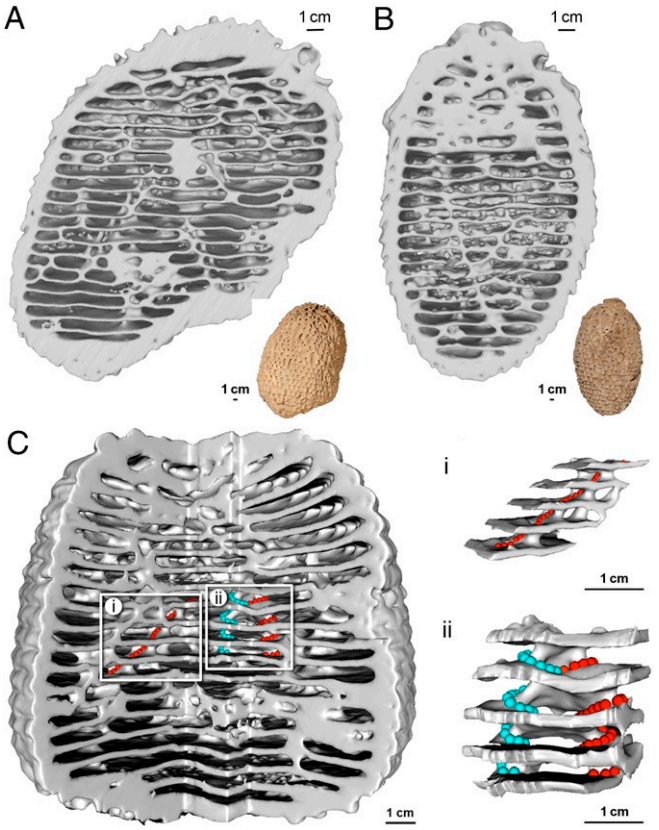

Fig. 1. Digital reconstruction of *A. lamani* nests reveals layered floors and chambers connected by linear and helicoidal ramps. (*A* and *B*) Cutaway view of two *A. lamani* nests, collected around Libreville (Gabon): MeMo14 (*A*) and MeMo13 (*B*). The nests were digitized with X-ray computer tomography and reconstructed in three dimensions (3D). (*C*) A large *A. lamani* nest (*Left*, MeMo80) collected in 2008 near Pointe Noire (Republic of the Congo) with examples of a linear ramp (*C*, *i*, red dots) and two helicoidal ramps with opposing chirality (*C*, *ii*, red and cyan dots).

were collected near Libreville, Gabon (*SI Appendix*, Fig. S1), although one of these (MeMo13) showed too much internal damage for a statistical analysis. A third nest (MeMo80, Fig. 1*C*) was collected in 2008 near Pointe Noire in the Republic of the Congo (*SI Appendix*, Fig. S1); in this nest, we measured that workers had length 4 to 5 mm and height 2 to 3 mm, while soldiers had length 8 to 10 mm with a height of 2 to 3 mm (12) (*SI Appendix*, Table S1). We digitized and imaged the excavated nests with a medical X-ray computed-tomography (CT) scanner (*Materials and Methods*), allowing for nondestructive exploration of the complete three-dimensional internal structure of each nest (Movie S1).

Both nests showed a similar external appearance and, based on our X-ray CT scans, also shared a similar internal architecture consisting of many floor layers arranged in parallel, with several vertical pillars connecting adjacent floors (Fig. 1 *A* and *B*). To investigate these structures, we systematically searched our two digitized examples for open corridors connecting floors (*Materials and Methods*), and we identified several occurrences of two types of ramps (Fig. 1*C*): linear ramps (15 in MeMo80 and 23 in MeMo14), in which a path connects floors along a linear incline, and helicoidal ramps (5 in MeMo80), in which the path spirals around a central pillar as it spans floors. The helicoidal ramps had no clearly preferred chirality (three left, two right), although a pair of co-occurring left-handed and right-handed helicoidal ramps was identified (Fig. 1 *C*, *ii*).

We then examined the internal architecture of the two *A. lamani* nests (MeMo80 and MeMo14; *SI Appendix*, Table S1) for which we had data, to quantify the spacing and arrangement of floors and ramps. For each nest, we assembled a series of 359 and 177 vertical slices, respectively (Fig. 2*A*), and measured the thickness of each floor and the vertical spacing between floors (Fig. 2*B*). In total, our dataset included 35 floors (17 in MeMo80 and 18 in MeMo14), sufficient to conduct separate analyses on each of the two nests. The floor thickness was on average 1.7 mm (median = 1.6 mm) in nest MeMo80 and on average 1.8 mm (median = 1.2 mm) in nest MeMo14. The floor spacing was on average 4.6 mm (median = 4.7 mm) in nest MeMo80 and on average 7.2 mm (median = 7.7 mm) in nest MeMo14. For both nests, the variance in floor thickness was low (coefficient of variation [CV] = 0.31 in MeMo80, CV = 0.59 in MeMo14), as was the variance in floor spacing (CV = 0.19 in MeMo80, CV = 0.22 in MeMo14), demonstrating that the flooring of the termite nests is arranged at regular vertical frequencies, with a strong continuity between adjacent floors (*SI Appendix*, Fig. S1 *B* and *C*).

Given this consistent arrangement of floors, we next investigated the positioning of ramps within the nests by measuring the horizontal distance from each ramp to the nearest ramp on the same floor (Fig. 2*C*). In MeMo80, we found a mean same-floor distance of 27.4 mm (median = 25.4 mm, CV = 0.41), and in MeMo14 this mean distance was 25.7 mm (median = 27.1 mm, CV = 0.33); these both deviated from a null model of randomly scattered ramps (Kolmogorov–Smirnov [KS] test, $P = 0.047$ for MeMo80, $P = 0.022$ for MeMo14; *SI Appendix*). We compared these measurements with the horizontal distance between ramps on adjacent floors. Because these ramps were often directly connected, this distance was much smaller for both nests, with a mean of 12.9 mm (median = 9.2 mm, CV = 0.79) in MeMo80 and a mean of 7.1 mm (median = 6.5 mm, CV = 0.47) in MeMo14, deviating in the opposite direction from the null model (KS test, $P = 0.046$ for MeMo80, $P = 0.040$ for MeMo14). Hence, while ramps tended to be spaced at fairly large, regular intervals across a floor, they tended to be positioned near ramps on adjacent floors, allowing for efficient vertical traversal between nest levels.

A Minimal Model of Biotectonics

To address how these structures are formed, we turn to a series of observations, old and new, to motivate a minimal continuum model of nest construction. With no evidence of design or a designer, termites build in response to local cues such as the nearby mound structure and secreted pheromones (17, 20). The resulting architecture both enables and constrains the movement of pheromones and termites and thereby modifies behavior, so that nest construction can be seen as a result of a feedback loop linking physical and behavioral dynamics (Fig. 3*A*). The architecture of the nest dictates which spaces are accessible to termite workers, the density of termite workers in turn controls the concentration of secreted pheromone, and the information carried by the pheromone profile in turn serves as a template for the ongoing remodeling of the nest architecture, thereby completing the feedback loop of nest morphogenesis.

We therefore model the spatiotemporal dynamics of three fields that depend on location denoted by the vector $\mathbf{x}$ and time t: the nest material density $u(\mathbf{x}, t)$, scaled from no nest material ($u = 0$) to fully compacted ($u = 1$), as well as the termite worker density $n(\mathbf{x}, t)$ and the pheromone concentration $\rho(\mathbf{x}, t)$, both in units of mass per volume. These three fields jointly evolve according to a set of conservation laws, expressed as the following differential equations (*SI Appendix*) for the nest material, termite workers, and pheromone levels:

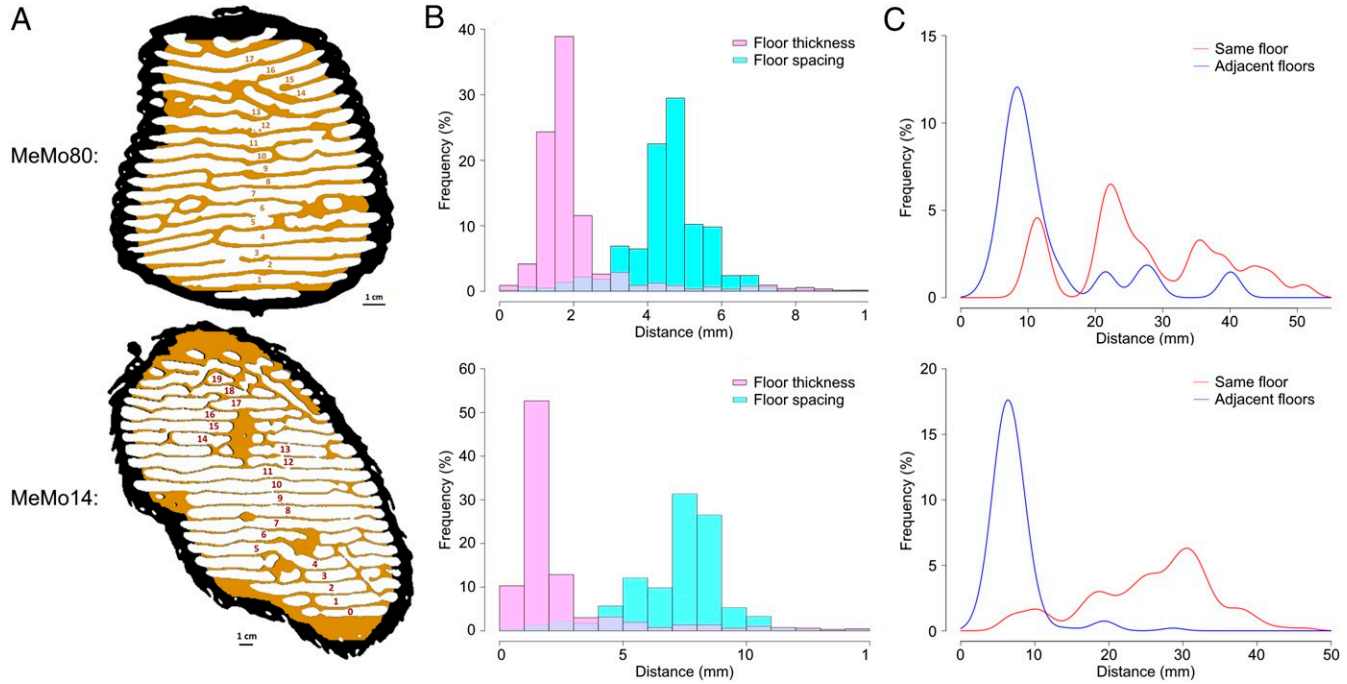

Fig. 2. Statistical analysis of *A. lamani* nests shows consistent floor and ramp spacing. (*A–C*, *Top*) Nest MeMo80. (*A–C*, *Bottom*) Nest MeMo14. (*A*) Representative vertical slices of nest structure with floors labeled in average height order. (*B*) Histograms for floor thickness (pink) and spacing between floors (cyan), measured in millimeters, corresponding to the nest depicted in *A*. Both the thickness of and spacing between floors tend to fall within a consistent band in each nest. (*C*) Density plot for the horizontal distance from a ramp to the nearest other ramp on the same floor (red) or on an adjacent floor above or below (blue), corresponding to the nest depicted in *A*. Ramps on the same floor tend to be spaced out, while ramps on adjacent floors often connect directly, resulting in minimal spacing.

$$\text{Nest material: } \partial_t u = \partial_z\,[g\partial_z u] + f_+ - f_-, \quad [1]$$

$$\text{Termite workers: } \partial_t n_\pm = \nabla\cdot[(1-u)D\nabla n_\pm + \chi n_\pm \nabla u] \pm (f_- - f_+)k^{-1}, \quad [2]$$

$$\text{Pheromone: } \partial_t \rho = \nabla\cdot[\delta\nabla\rho] + Hf_+ - \gamma\rho, \quad [3]$$

where ∂_t and ∂_z are the differential operators in time and height, respectively; $\nabla\cdot$ is the three-dimensional divergence operator; and ∇ is the three-dimensional gradient operator. Here Eq. **1** reflects the addition and removal of the nest material, with f_+ and f_- denoting the building and removal rates of dirt (whose functional form is discussed below). Moreover, the poroelastic diffusivity of dirt g captures its capacity to settle under the influence of gravity (21); this term breaks the rotational symmetry of the model equations and establishes a defined vertical orientation for the nest. Eq. **2** reflects the dynamics of termites carrying dirt n_+ or not carrying dirt n_-, with a flux that has two components: an effective diffusivity that is proportional to the amount of open space, i.e., $(1-u)D$, as well as a chemotactic term that drives termite workers into open and low-density nest regions with chemotactic coefficient χ (22, 23). The final term represents switching between n_+ and n_-, with the pellet size k denoting the average amount of dirt transported by a worker. Finally, Eq. **3** reflects the dynamics of pheromones as they diffuse with a diffusion coefficient δ, are secreted into deposited soil at a level H per pellet (19), and degrade through evaporation at a rate γ. We note that the pheromone is relatively nonvolatile and thus not advected by the ambient fluid, since the subterranean nests of *Apicotermes* do not typically have noticeable temperature gradients (24).

To complete the formulation of our model, we require functional forms for the building rate f_+ and removal rate f_-. Although these rates have not been directly measured in *A. lamani* termites, the building rate has been investigated for the neotropical termite *Procornitermes araujoi* (25), and both rates have also been quantified in the ant *L. niger* (19). In all cases, we find that the local nest density scales directly with the building rate and inversely with the removal rate, resulting in high-density regions becoming increasingly compacted while low-density regions are excavated. Moreover, this positive feedback is mediated by a pheromone added by the workers to the building material (Fig. 3*B*), so that the termites are more likely to deposit dirt in regions marked by pheromone as being sites of active remodeling and so that building does not take place either where there is no nest material ($u=0$) or where the nest material is already fully compacted ($u=1$). It is reasonable also that the removal rate scales with the density of termite workers not carrying dirt and with the density of dirt u available for removal. Given these basic considerations, the simplest possible functional forms for f_+ and f_- are

$$\text{Building rate: } f_+ = r_+ n_+ \rho u(1-u), \quad [4]$$

$$\text{Removal rate: } f_- = r_- n_- u, \quad [5]$$

where $r_\pm$ are rate constants. With these choices, the dynamics of nest morphogenesis as described by our model can be captured by only a small number of nondimensional parameters: the scaled pheromone potency Hr_+/r_-; the scaled evaporative flux γ/r_-; the pellet size k; and the scaled diffusivities δ/D, χ/D, and g/D (*SI Appendix*). For simplicity, and to directly study the self-contained organization of this system, we model the nest as a closed three-dimensional domain, using no-flux boundary conditions, such that when integrated over the nest domain the total number of termites $|n|$ and the total quantity of dirt u are conserved. With this formulation, our model describes the simultaneous disassembly and reassembly of the nest, which are features of both initial nest construction and its ongoing renovation during its lifespan (19).

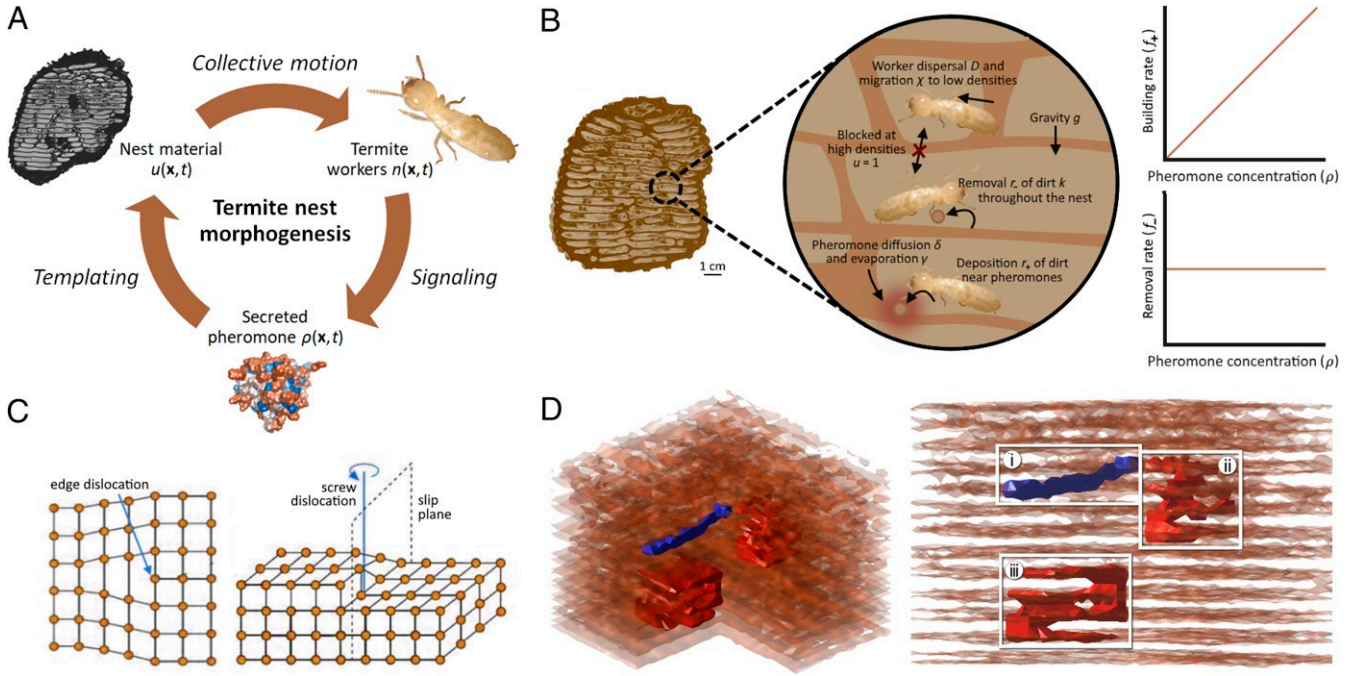

Fig. 3. Biotectonic model predicts floor spacing and ramp emergence in termite nests. (*A*) Model schematic of the feedback loop driving nest construction, highlighting the interactions between nest material u, termite workers n, and secreted pheromone ρ. (*B*) Illustration of a local region of a nest, showing the processes in our model. Termite workers migrate preferentially to low-density regions and cannot travel through very high-density regions. Workers remove dirt throughout the nest but are more likely to deposit dirt near pheromones which they release during deposition. Pheromones are assumed to have a low diffusivity and hence provide a local signal. (*C*) Diagrams of edge and screw dislocations in floor patterning. Edge dislocations that result from floor misalignment can give rise to linear ramps, while screw dislocations can lead to helicoidal ramps that pivot about a slip plane. (*D*) Three-dimensional reconstruction of a nest simulated according to our construction model, shown here at two angles. This simulated nest contains one linear ramp (*i*, blue) and two helicoidal ramps (*ii* and *iii*, red).

Natural Patterns in Simulated Nests

We conducted 500 independent simulations of nest construction by initializing our model each time with uniform nest density $u(\mathbf{x}, t)$ and pheromone concentration $\rho(\mathbf{x}, t)$, and with a randomly dispersed density of termite workers $n(\mathbf{x}, t)$, using measured and inferred parameter values from several studies on termite nest structure and behavior (*SI Appendix*, Table S2) and a numerical implementation of a stable Euler differencing scheme (*Materials and Methods*) run until a steady-state distribution of floor thickness and separation is achieved. Nest construction time ranged from 25.5 to 94.6 d (95% confidence interval; *SI Appendix*, Fig. S6). The model generated simulated nests (*SI Appendix*, Fig. S3 *A–C*) with regularly spaced floors of roughly planar orientation (orthogonal to the direction of gravity in the model) and a floor thickness that scales as $(\delta/\gamma)^{1/2}$ in some regimes (*Materials and Methods* and *SI Appendix*, Fig. S3*D*). For a pheromone diffusivity $\delta = 100\ \mu m^2/s$ and an intermediate degradation rate $\gamma = 1.0/h$, this gives an average prediction of a 1.74-mm floor thickness, in line with our observed measurements of 1.7 and 1.8 mm in MeMo80 and MeMo14, respectively. To evaluate model sensitivity, we also allow all parameters to vary across realistic ranges (*SI Appendix*, Table S2)—including three orders of magnitude for the degradation rate γ, as this value is the most variable in the literature (19). Across all parameter ranges, we observed floor thicknesses in the relatively constrained range 1.2 to 2.5 mm, with the greatest sensitivity to changes in the diffusivity δ and degradation rate γ as predicted by our scaling analysis (*SI Appendix*, Fig. S4).

Our simulated nests contained surface edges (topological defects, Fig. 3*C*) spanning across floors and sometimes forming traversable connections (Fig. 3*D*) corresponding to linear ramps—in which one floor terminates to provide the vertical space necessary for a simple ramp between adjacent floors—and helicoidal ramps, which wind about a vertical pillar that serves as a dislocation line spanning multiple floors (26) (*SI Appendix*, Fig. S5). By identifying the eventual location of a ramp, we observe the dynamical process by which ramps emerge from these defects during the construction process (Fig. 4*A*). Ramps first arise from regularly spaced floors in adjacent nest regions that are misaligned at the boundary via edge dislocation (in which an intermediate floor terminates at the boundary), which are connected to form a linear ramp to the floors above or below, or via screw dislocation (rotational misalignment about a slip plane), providing the axis of rotation about which a helicoidal ramp can be built (Fig. 3*C*). This misalignment of floor spacing is required for ramp formation; in follow-up simulations that initialized the mound with perfect floor regularity, ramps were altogether absent (*SI Appendix*). Moreover, when varying our model parameters, we find that two parameters control whether helicoidal ramps form at steady state: the scaled pheromone potency Hr_+/r_- and the scaled pheromone evaporation rate γ/r_-, yielding a phase space for their emergence (Fig. 4*B*). This is consistent with previous agent-based simulations of ant nest construction that pointed to the central role of the pheromone evaporation rate in influencing nest structures (19).

A fly-through of our simulated nests (Movie S2) reveals the structural similarity of the simulated nests produced by our model with the scanned *A. lamani* nests. To quantitatively evaluate this similarity, we gathered an identical set of statistics to describe the simulated nest topologies. We found that floor thickness and spacing between floors were similarly consistent in both the simulated and scanned nests, indicated by distributions with a similarly narrow variance (Fig. 4*C*). Moreover, the horizontal spacing between neighboring ramps on the same floor was

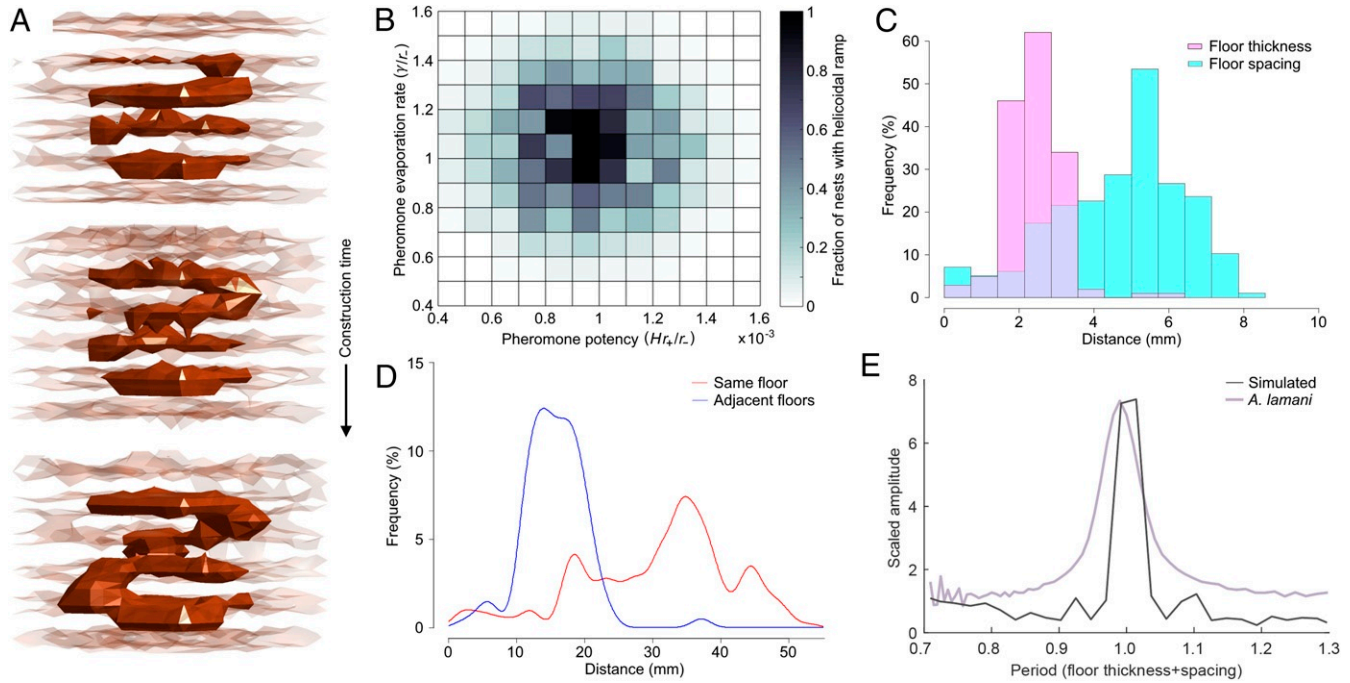

Fig. 4. Simulated nests resemble natural *A. lamani* nests and produce helicoidal ramps across a range of parameters. (*A*) Time snapshots of helicoidal ramp emergence during simulated nest construction, from early (*Top*) to late (*Bottom*) in the building period. (*B*) Heatplot for the frequency of helicoidal ramps in a simulated nest as a function of the two model parameters governing pheromone dynamics. (*C*) Histograms for floor thickness (pink) and spacing between floors (cyan), as measured in millimeters, averaged over simulated nests. The histograms show a pattern similar to the natural nests in Fig. 2*B*. (*D*) Density plot for the horizontal distance from a ramp to the nearest other ramp on the same floor (red) or on an adjacent floor above or below (blue), averaged over simulated nests and resembling the natural patterns shown in Fig. 2*C*. (*E*) The power spectrum of nest density, averaged over horizontal slices, peaks sharply at a one-floor period for both simulated (gray) and natural (purple) nests, indicating regularly spaced floor structures.

greater than the horizontal spacing between ramps on adjacent floors that often connected directly, as observed in the scanned nests (Fig. 4*D*). To assess the similarity of the simulated and scanned nests on large scales, we carried out a spectral analysis of the average nest density as a function of height for both the scanned and simulated nests and found that these density profiles are very similar (Fig. 4*E*). Together, these metrics indicate that the simulated nests resemble natural nests across global and local scales.

Emergent Biotectonics from Physics and Behavior

Our minimal theoretical framework links three spatiotemporal fields involved in the biotectonics of termite nests: dirt to constitute the nest, termite workers to shape the nest, and secreted pheromone to mark active regions of the nest. They allow us to capture two key geometrical and topological features of termite nests, namely the regular vertical spacing of floors and the horizontal spacing of ramps on the same or adjacent floors, as well as the months-long timing of the nest construction process (12). This feedback loop involving architecture, behavior, and information that drives nest construction is quite general in biological systems; relatedly, it is implicated also in the macromorphogenesis of termite mounds (18) and might provide insight into emergence of other animal architectures, such as ant nests or mounds and nests of other termite subfamilies (1, 19, 27). Understanding the complex ways in which these systems differ, while still adhering to the same fundamental principles, is a task for the future. Nevertheless, our finding that key termite nest structures emerge spontaneously in our model for a range of parameter values points to it being a nonequilibrium steady state that is robust and adaptable—a direct consequence of the ability of a colony to both lay down and respond to cues in its environment.

An important open question is the role of heat gradients and airflow within the nest (5, 6, 15), which are determined by the nest structure and in turn help to propagate pheromones and other signals, such as carbon dioxide levels (28). Although the diffusion rate of pheromones can range widely depending on their molecular weight and chemical properties, the pheromones we consider here have low diffusivities (20), and thus only provide a localized signal useful in nest construction. Given these low diffusivities, heat-driven airflow would result in a negligible change when incorporated into our model (*SI Appendix*, Fig. S6), although other potential odors with a higher diffusivity, such as those secreted by the queen, would be more susceptible to internal nest flow and hence more important to the larger-scale problem of the global templating and emergence of overall mound shape (18, 20). In the subterranean nests of *Apicotermes*, we expect that the role of heat gradients and airflow is minor relative to that in above-ground nests which are directly subjected to sunlight and air currents. Furthermore, because termite workers can move with relative ease through each nest, the initial dispersion pattern of workers within the nest would have minimal effect on the overall nest structure (*SI Appendix*, Fig. S7).

In constructing the functional, palatial structures of their nests, termites demonstrate a remarkable capacity for spontaneous self-organization through stigmergic interactions, coupling their behavior to deposited cues in their local environment—a process that stands in stark contrast to the planned building processes that give rise to human architecture. By studying the natural architectures that termites and other insects build and inhabit, and by understanding their ability to leverage their surroundings for information transfer, we can better understand how multiagent system approaches can be adapted for our own lives, from swarm intelligence to architectural design (29). After all, while we as humans have a mere ∼400,000 y of experience with

constructing primitive structures (30), mound-building termites of the family Termitidae have spent close to 50 million y (31) developing one of the grandest examples of architecture in the natural world.

Materials and Methods

X-Ray CT. Each nest was imaged using X-ray computed tomography with a medical scanner and reconstructed into a series of virtual cuts (512 × 512 pixels). MeMo13 and MeMo14 were scanned with a Somatom Sensation16 (Siemens) at Centre Hospitalier Universitaire (CHU) de Toulouse, Rangueil, France using exposure parameters of 120 kV and 150 mA, slice thickness of 1 mm, interslice distance 0.5 mm. MeMo80 was scanned with a LightSpeed Ultra (GE Medical Systems) at CHU Dijon using exposure parameters 100 kV and 170 mA, slice thickness of 0.625 mm, interslice distance 0.3 mm. Reconstruction of the virtual cuts (Fig. 1) was performed in the open-source software Horos (GNU Lesser General Public License, Version 3).

Investigation of Internal Structures. Ramps (with connecting holes to the floor above) and pillars (supporting the above floor without a passway) were identified by visual inspection of three orthogonal planes at each voxel of the original CT. For helices, identification was confirmed by reconstructing a perspective surface rendering (e.g., Fig. 1*C*). Mean coordinates for the base of each ramp or pillar were extracted (Fig. 2*A*) for the statistics in Fig. 2*C* and *SI Appendix*, Table S1. For Fig. 2*B*, MeMo14 was rotated to align horizontal floors with the *xy* plane with bilinear interpolation. The outer walls were removed from binarized images by first dilating each slice five times to close all outside openings and then defining an outline ROI of the nest, used to compute nest volume. All pixels outside the new ROIs were removed to obtain nests without outer walls as in Fig. 2*A*.

Floor thickness and floor spacing were measured by counting the number of consecutive black or white pixels in each vertical pixel line of the stacked images. The presence of pillars/ramps led to heavy right tails in both distributions, removed by cutting off all measures above twice the median floor height and alpha trimming the resulting distributions with $\alpha = 0.02$ on both sides. To check for the continuation of ramps across several floors, we selected for each floor the horizontal slice for which the horizontal pixel density was minimal (*SI Appendix*, Fig. S1*B*), computed the correlation coefficient between the pixels of adjacent floors, and compared them to the correlation coefficients between slices at least three floors separated (*SI Appendix*, Fig. S1*C*).

Numerical Solution of Model Equations. To simulate our construction model, we implemented a finite difference solver to numerically integrate the system of Eqs. **1**–**5**. We initialized each simulation with uniform nest density $u = 0.5$ (halfway packed) and uniform pheromone concentration $\rho = 0.1\,\mathrm{ng/cm^3}$, and with randomly scattered termite workers, such that the density of termites n at each grid location x was drawn from an exponential distribution with nondimensional mean 0.1. At each time step, the gradient and Laplacian of each of the three fields were calculated using second-order differencing in space, and the nest interior was then updated with first-order differencing in time. For each set of model parameters, 500 independent simulations were conducted.

Data Availability. The HTML three-dimensional images and Datasets S1 and S2 have been deposited in Harvard Dataverse (https://doi.org/10.7910/DVN/Z1GWTI) (32).

ACKNOWLEDGMENTS. We thank A. Robert for providing nest MeMo80 and the natural history museum in Paris for providing nests MeMo13 and MeMo14, both collected by P. P. Grassé. We are indebted to our reviewers for their careful reading and insightful suggestions. This work was supported by NSF Grant DGE-1144152 (to A.H.), Agence Nationale de la Recherche Grant ANR-06-BYOS-0008 (to G.T.), a China Scholarship Council PhD Grant (to L.G.), and the NSF Physics of Living Systems Grant PHY1606895 (to L.M.).

1. M. Hansell, *Animal Architecture* (Oxford University Press, 2005).
2. A. Perna, G. Theraulaz, When social behavior is molded in clay: On growth and form of social insect nests. *J. Exp. Biol.* **220**, 83–91 (2017).
3. C. C. Lee, K. B. Neoh, C. Y. Lee, Caste composition and mound size of the subterranean termite macrotermes gilvus (isoptera: Termitidae: Macrotermitinae). *Ann. Entomol. Soc. Am.* **105**, 427–433 (2012).
4. J. S. Turner, On the mound of macrotermes michaelseni as an organ of respiratory gas exchange. *Physiol. Biochem. Zool.* **74**, 798–822 (2001).
5. H. King, S. A. Ocko, L. Mahadevan, Termite mounds harness diurnal temperature oscillations for ventilation. *Proc. Natl. Acad. Sci. U.S.A.* **112**, 11589–11593 (2015).
6. S. A. Ocko *et al.*, Solar-powered ventilation of African termite mounds. *J. Exp. Biol.* **22**, 3260–3269 (2017).
7. S Camazine *et al.*, *Self-Organization in Biological Systems* (Princeton University Press, 2003), vol. 7.
8. D. J. T. Sumpter, *Collective Animal Behavior* (Princeton University Press, 2010).
9. C. Anderson, D. W. McShea, Intermediate-level parts in insect societies: Adaptive structures that ants build away from the nest. *Insectes Soc.* **48**, 291–301 (2001).
10. T. J. Czaczkes, C. Grüter, F. L. W. Ratnieks, Trail pheromones: An integrative view of their role in social insect colony organization. *Annu. Rev. Entomol.* **60**, 581–599 (2015).
11. E. Bonabeau, G. Theraulaz, J. L. Deneubourg, S. Aron, S. Camazine. Self-organization in social insects. *Trends Ecol. Evol.* **12**, 188–193 (1997).
12. J. Desneux, A. E. Emerson, *Les Constructions Hypogées des Apicotermes Termites de l'Afrique Tropicale* (Musée Royale du Congo Belge, 1952), vol. 17.
13. R. S. Schmidt, Functions of apicotermes nests. *Insectes Soc.* **7**, 357–368 (1960).
14. J. Korb, K. E. Linsenmair, The architecture of termite mounds: A result of a trade-off between thermoregulation and gas exchange?. *Behav. Ecol.* **10**, 312–316 (1999).
15. K. Singh *et al.*, The architectural design of smart ventilation and drainage systems in termite nests. *Sci. Adv.* **5**, eaat8520 (2019).
16. G. Theraulaz, E. Bonabeau, A brief history of stigmergy. *Artif. Life* **5**, 97–116 (1999).
17. P. P. Grassé, La reconstruction du nid et les coordinations interindividuelles chez-bellicositermes natalensis et cubitermes sp. la théorie de la stigmergie: Essai d'interprétation du comportement des termites constructeurs. *Insectes Soc.* **6**, 41–80 (1959).
18. S. A. Ocko, A. Heyde, L. Mahadevan, Morphogenesis of termite mounds. *Proc. Natl. Acad. Sci. U.S.A.* **116**, 3379–3384 (2019).
19. A. Khuong *et al.*, Stigmergic construction and topochemical information shape ant nest architecture. *Proc. Natl. Acad. Sci. U.S.A.* **113**, 1303–1308 (2016).
20. O. H. Bruinsma. "An analysis of building behavior of the termite macrotermes subhyalinus (Rambur)," PhD thesis Landbouwhogeschool Wageningen, Wageningen, The Netherlands, (1979).
21. M. A. Biot, General theory of three-dimensional consolidation. *J. Appl. Phys.* **12**, 155–164 (1941).
22. A. Stevens, The derivation of chemotaxis equations as limit dynamics of moderately interacting stochastic many-particle systems. *SIAM J. Appl. Math.* **61**, 183–212 (2000).
23. P. Amorim, Modeling ant foraging: A chemotaxis approach with pheromones and trail formation. *J. Theor. Biol.* **385**, 160–173 (2015).
24. R. S. Schmidt, Apticotermes nests. *Am. Zoologist* **4**, 221–225 (1964).
25. D. Fouquet, A. M. Costa-Leonardo, R. Fournier, S. Blanco, C. Jost, Coordination of construction behavior in the termite Procornitermes araujoi: Structure is a stronger stimulus than volatile marking. *Insectes Soc.* **61**, 253–264 (2014).
26. J. P. Hirth, J. Lothe, T. Mura, *Theory of Dislocations* (Cambridge University Press, 1983).
27. A. Perna *et al.*, Topological efficiency in three-dimensional gallery networks of termite nests. *Physica A* **387**, 6235–6244 (2008).
28. M. D. Cox, G. B. Blanchard, Gaseous templates in ant nests. *J. Theor. Biol.* **204**, 223–238 (2000).
29. J. S. Turner, R. C. Soar, "Beyond biomimicry: What termites can tell us about realizing the living building" in *Industrialised, Integrated, Intelligent sustainable Construction: I3CON Handbook 2*, I. Wallis, L. Bilan, M. Smith, A. S. Kazi, Eds. (I3CON & BSRIA Limited, Bracknell, UK, 2010), pp. 234–248.
30. P. Villa, *Terra Amata and the Middle Pleistocene Archeological Record of Southern France* (University of California Publications in Anthropology, Berkeley, CA, 1983), vol. 13.
31. D. A. Arab *et al.*, Parallel evolution of mound-building and grass-feeding in Australian nasute termites. *Biol. Lett.* **13**, 20160665 (2017).
32. A. Heyde, L. Guo, C. Jost, G. Theraulaz, L. Mahadevan, Termite biotectonics data. Harvard Dataverse. https://doi.org/10.7910/DVN/Z1GWTI. Deposited 12 November 2020.